Mesostructuring in Liquid-Liquid Extraction Organic Phases Originating from Critical Points

Michael J. Servis*,† and G. B. Stephenson‡

†*Chemical Sciences and Engineering Division, Argonne National Laboratory, Lemont, IL 60439*

‡*Materials Science Division, Argonne National Laboratory, Lemont, IL 60439, USA*

E-mail: mservis@anl.gov

Abstract

Organic phase structure plays an important role in solute extraction energetics and phase behavior of liquid-liquid extraction (LLE) systems. For a binary extractant (amphiphile)/solvent mixture of relevance to LLE, we find that the organic phase mesostructuring is consistent with extractant concentration fluctuations as the compositional isotherm traverses the Widom line above its liquid-liquid critical point. This reveals a different mechanism for the well-documented heterogeneities in LLE organic phases that are typically attributed to micellization.

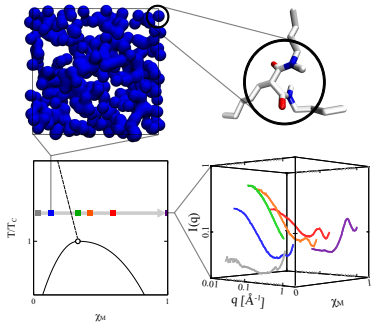

Liquid-liquid extraction (LLE) is a chemical process used for the selective recovery of target materials from complex chemical matrices, such as metals from dissolved ores.[1] The distribution of components between immiscible liquid phases, such as oil and water, is driven by differences in solvation free energy between the two phases. Polar components are transferred to the nonpolar organic phase by complexation with amphiphilic "extractant" molecules. Given that effective separations often operate on relatively small free energy differences between phases, including on the order of thermal energy, minor energetic contributions are relevant for modeling and designing successful separations processes. Among such contributions are those originating from the mesoscale structure of the oil phase, driven by aggregation of the amphiphilic extractant molecules and extracted polar solutes.[2–6] Organic phase aggregation also impacts third phase formation, which is a deleterious, efficiency limiting phenomenon wherein the organic phase becomes sufficiently loaded with extracted polar components that the amphiphile/solute aggregates are no longer soluble in the organic solvent. The organic phase then splits into "light" and "heavy" phases, the latter of which contains the majority of extracted species.[7–10]

Despite its importance for process design, the fundamental drivers of organic phase mesostructure are poorly understood. In this study, we consider a simplified binary extractant/solvent mixture without extracted water or aqueous solutes whose behavior is relevant to more complex systems. Generally, LLE systems are treated as microemulsions, where the amphiphilic extractant molecules form reverse micelles in the organic phase with aqueous constituents extracted into their polar cores.[2,7] The primary evidence for this description is the small angle X-ray scattering (SAXS) behavior of the organic phase at low scattering vector, q, which is consistent with scattering patterns expected for reverse micellar systems. The mesostructure of the organic phase is typically quantified by fitting small angle scattering patterns with colloidal models representing those reverse micelles.[2,7,11,12] However, it was recently reported that a series of binary malonamide extractant/alkane solvent organic phases show the scattering features typically attributed to micellization despite a lack of

water (or other polar solutes) or any microemulsion-like nanostructure.[13] This suggests a new—or complementary—explanation of organic phase mesostructure may be needed.

In this study, we propose that the structure evident in SAXS comes from concentration fluctuations related to the critical point of the binary malonamide/alkane mixture. While LLE systems contain aqueous and organic phases, here we consider just the organic phase, such that demixing of the organic phase into two phases is analogous to third phase formation. The so-called Widom line is the locus of maxima of the correlation length, ξ, emanating from the critical point into the single phase region, as illustrated in Figure 1. The correlation length diverges at the critical point while the strength of its maximum along the Widom line decays with increasing temperature above the critical temperature, T_C. The Widom line has been identified for liquid-vapor critical points in single-component systems for small molecules[14–16] and model potentials[17,18] as well as for the liquid-liquid critical points (LLCPs)[19] including supercooled water.[20–25] Compared to liquid-vapor critical points, LLCPs more often occur near ambient conditions and the effects of the critical point on thermodynamic properties of the solution extend farther from the critical point.[26,27] Therefore, we might expect a similar behavior of the correlation length for an isotherm spanning the amphiphile concentration range in the single phase region for the binary mixture studied here: *N*,*N*'-dimethyl,*N*,*N*'-dibutylpentylmalonamide (DMDBPMA)/*n*-dodecane.

Here, we choose DMDBPMA for its reduced lipophilicity and resulting proximity to the third phase formation phase boundary: the DMDBPMA/*n*-dodecane organic phase splits simply upon contact with water over a wide extractant concentration range.[28,29] Self-association of DMDBPMA in *n*-dodecane is consistent with commonly used malonamide extractants featuring longer alkyl tails and increased lipophilicity, including *N*,*N*'-dimethyl,*N*,*N*'-dibutyltetradecylmalonamide (DMDBTDMA).[13] Therefore, the conclusions drawn here about DMDBPMA/alkane binary mixtures are expected to apply to other malonamides; the scattering features observed for DMDBPMA are analogous as well to those of other malonamide extractants.[13] In this study, we combine molecular dynamics (MD)

simulations (see Supporting Information) with SAXS data from ref. 28 to demonstrate that the electron density fluctuations observed for these systems in the low-q scattering region are consistent with critical fluctuations manifested away from the LLCP rather than micellization.

The compositional isotherm at room temperature is defined by DMDBPMA mole fraction, χ_{M}. Figure 1 shows the trends in simulation structures and experimental SAXS patterns[28] along that isotherm. With increasing DMDBPMA concentration, the SAXS peak near $q \approx 0.6$ Å, which results from alkyl tail spacing of the malonamide head groups,[13] increases as the solution becomes more densely packed. The low-q intensities that result from the long-range fluctuations in malonamide concentration increase with concentration at low χ_{M} before decreasing after $\chi_{\mathrm{M}} = 0.33$. The experimental SAXS data[28] are compared to SAXS patterns calculated from the corresponding simulation trajectories in Figure 2. (Patterns for the remaining simulations are given in the Supporting Information.) The good overall agreement in the SAXS trends between the experiment and simulations lend confidence to the interpretation of solution structure from the simulations. The agreement is worst at $\chi_{\mathrm{M}} = 0.42$, particularly in the low-q region. We suspect this is a finite size effect: doubling the linear dimension of the simulation box for that mole fraction significantly improves the low-q behavior of the simulation SAXS pattern.

Amphiphile organization is evident from the simulation trajectories, with snapshots for three systems shown in Figure 1. At low concentration, DMDBPMA monomers dominate, with only a small degree of self-association. For moderate, process-relevant concentrations, significant malonamide aggregation occurs and solution heterogeneity is visually apparent. At high concentration, polar regions of DMDBPMA head groups and nonpolar regions of aliphatic tails and solvent are interspersed in a bicontinuous-like fashion. Malonamide self-association is quantified by cluster analysis, an intuitive description of amphiphile aggregation that is accessible from simulation trajectories,[13,30–34] described in the Supporting Information. Cluster size distributions are plotted in Figure 3. At low DMDBPMA concentration,

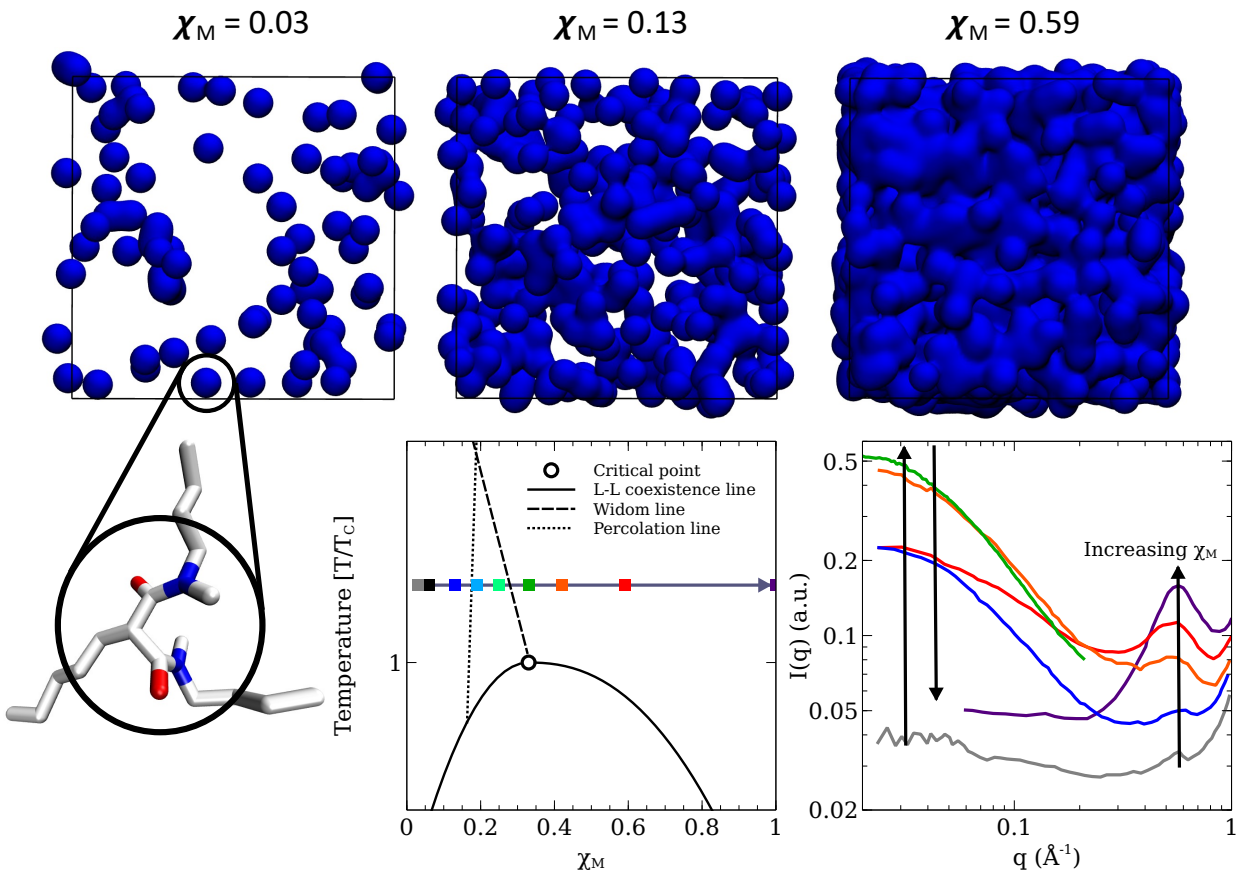

Figure 1: On the top row, snapshots are shown for $\chi_{\mathrm{M}} = 0.03$, 0.13 and 0.59 simulations. Surface representations of the malonamide molecules are drawn in blue, using the amide-bridging carbon atom positions, with solvent omitted for clarity. A snapshot of a DMDBPMA molecule is shown below, with nitrogen atoms drawn in blue, oxygen in red and carbon in white with hydrogen atoms not depicted. On the bottom left plot, the compositional isotherm studied here is shown with relevant features of the phase diagram. The relative positions of the critical point, reduced temperature of the isotherm, liquid-liquid coexistence curve, Widom line and percolation line are schematic. The bottom right plot shows SAXS patterns along the isotherm (from Bauduin et al.[28]) with arrows highlighting trends in the scattering features with increasing χ_{M}.

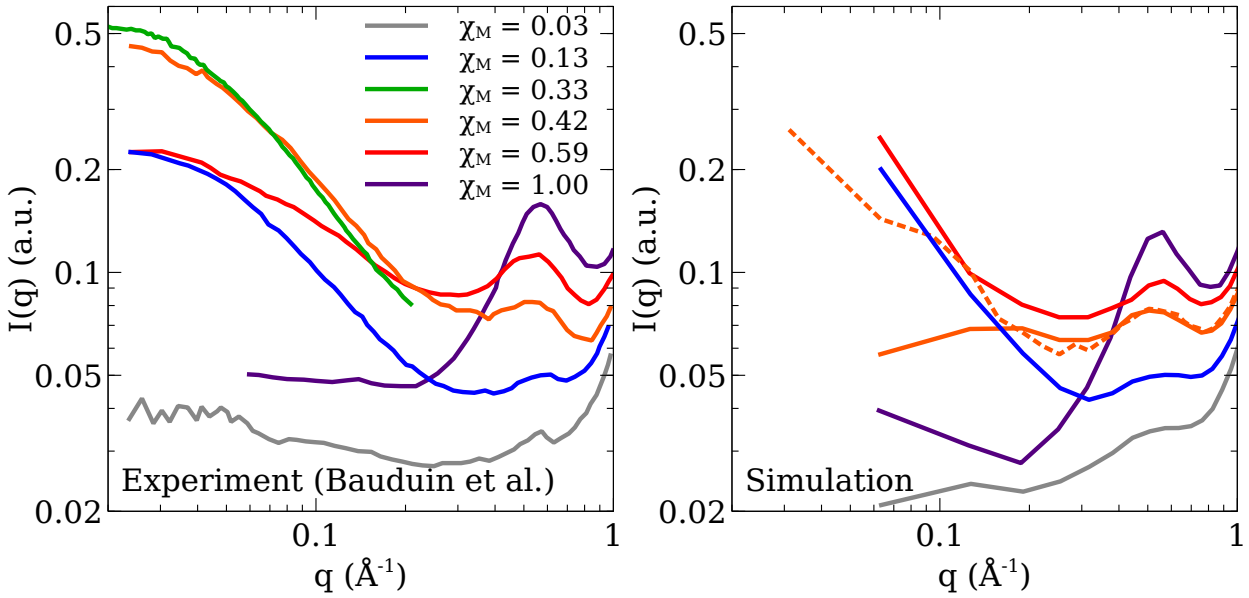

Figure 2: Experimental SAXS patterns from Bauduin et al.[28] (left) are compared to SAXS data calculated from simulation trajectories (right). Simulation data for 10 nm periodic cubic box lengths are drawn with solid lines, and data for the 20 nm box length with a dashed line.

the cluster sizes are exponentially distributed. Then, near $\chi_M = 0.19$, the distribution transitions to a power law. These power law distributions have slopes that are consistent with percolation of the DMDBPMA network: overlayed on the cluster size distributions in Figure 3 is a power law distribution with the percolation Fisher exponent, $\tau = 2.19$, for the cluster size distribution in three dimensions.[35] After increasing χ_M further, the system-spanning cluster dominates, manifested as a narrow peak at large cluster size, in dynamic equilibrium with small, discrete clusters.

Cluster analysis reveals a lack of any distinct microemulsion-like structures that would have a characteristic aggregate size, which would manifest as a maximum in the distribution at the associated cluster number.[36] For this system, colloidal model fitting has suggested aggregate numbers of 3-4.[28] Instead, continuous transitions in clustering and SAXS features are observed between exponential and power law distributions that lack such characteristic cluster numbers, with the only maxima corresponding to the spanning cluster in percolating systems. This is consistent with the lack of clear critical aggregation concentrations in

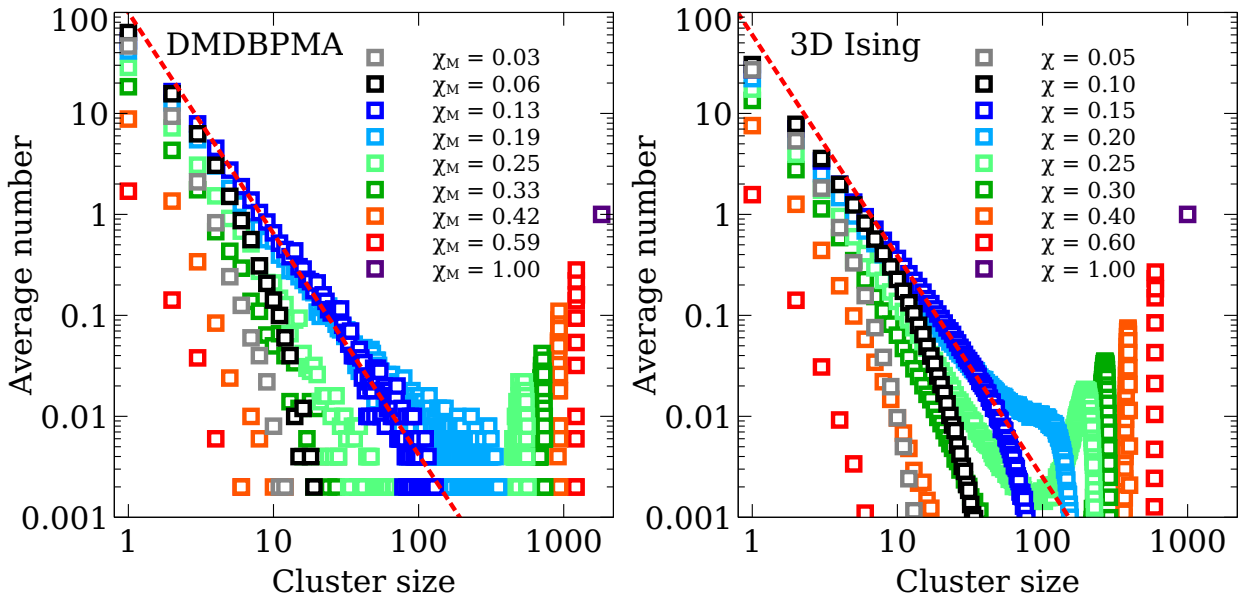

Figure 3: The left plot shows the DMDBPMA cluster size distributions for each DMDBPMA mole fraction. On the right, the cluster size distributions are plotted for the 3D Ising model on a simple cubic lattice for different fractions of spin up sites. A power law distribution with the Fisher exponent $\tau = 2.19$ is overlayed with a dotted red line.

malonamide organic phases.[3] We find that malonamide aggregation in these systems are more analogous to clustering in the 3D Ising model (details of calculations in Supporting Information). Figure 3 shows cluster size distributions of one spin type for the 3D Ising model on a simple cubic lattice with fixed spin fractions, with fractions of that spin type varied along an isotherm above the critical temperature. Across the series of fixed spin up fractions—in analogy to the series of DMDBPMA mole fractions—we observe remarkably similar cluster size distributions, demonstrating that DMDBPMA clustering is qualitatively captured by a simple correlated lattice model.

Given the lack of characteristic aggregate sizes, an alternative explanation for the long-range fluctuations observed at low-q in the SAXS data is needed. The SAXS intensity, $I(q)$, at low-q shows classical Ornstein-Zernike behavior,[37] described by

$$I(q) = \frac{I(0)}{1 + (q\xi_{\text{O-Z}})^2} + B, \tag{1}$$

where $\xi_{\text{O-Z}}$ is the Ornstein-Zernike correlation length, B is the background scattering. Deviation of the $(q\xi_{\text{O-Z}})^{2-\eta}$ exponent by η, the "dimensional anomaly" exponent,[38] is neglected. We plot this correlation length for each experimental SAXS profile in Figure 4 by fitting the scattering intensities at the low-q region, with fits shown in Figure S4. A maximum in the correlation length occurs between $\chi_{\text{M}} = 0.13$ and 0.33, before decaying slowly at higher mole fractions. This behavior of the correlation length is consistent with the isotherm traversing the single phase region above the critical point, as illustrated in Figure 1, with the isotherm crossing the Widom line at the maximal value of $\xi_{\text{O-Z}}$, between $\chi_{\text{M}} = 0.13$ and 0.33. The critical point is expected to occur at $\chi_{\text{M}} < 0.5$ due to the asymmetry in molar volumes of the binary DMDBPMA/n-dodecane mixture. Insofar as the Widom line is a continuation of the line of rectilinear diameters,[14,15] a negative slope in the $\chi_{\text{M}} - T$ phase diagram might be anticipated, as illustrated in Figure 1. Both of these are consistent with the χ_{M} range of the observed $\xi_{\text{O-Z}}$ maximum.

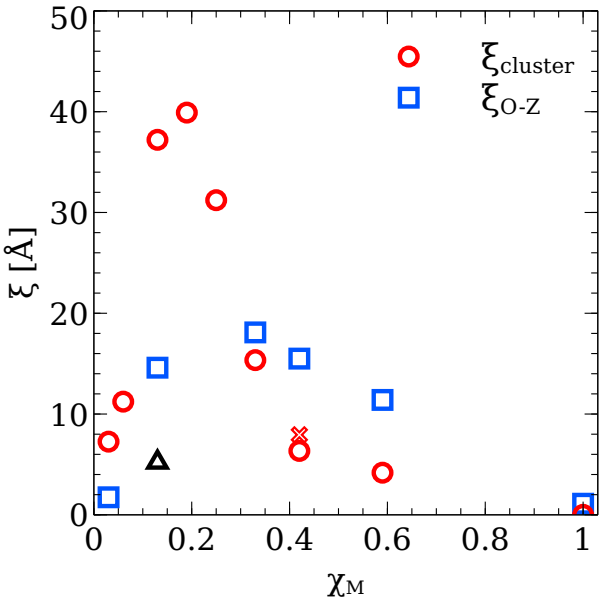

Figure 4: The SAXS Ornstein-Zernike ($\xi_{\text{O-Z}}$) (blue squares for DMDBPMA, black triangle for DMDBTDMA) and MD cluster (ξ_{cluster}) correlation lengths are plotted across the range of DMDBPMA mole fractions. The red cross corresponds to the 20 nm simulation box, and the red circles to the 10 nm simulation boxes.

A connection between the Ornstein-Zernike correlation length and simulation clustering

is desirable: it would link the former, an experimentally observable feature of interest, to the latter, a physically intuitive description of solution structure that is commonly applied to quantify extractant aggregation.[13,33,34] To that end, we compute a cluster correlation length, ξ_{cluster} from the malonamide clusters to qualitatively compare with $\xi_{\text{O-Z}}$. Here, ξ_{cluster} is defined for N total molecules by

$$\xi^2_{\text{cluster}} = \frac{\sum_{i<j}^{N}{}' \delta_{ij} r_{ij}^2}{\sum_{i<j}^{N}{}' \delta_{ij}}, \tag{2}$$

where r_{ij} is the distance between molecules i and j with δ_{ij} being unity if the molecules are on the same cluster and zero otherwise.[35] The prime denotes that when a spanning cluster is observed (for $\chi_{\text{M}} \geq 0.25$), the contribution of the largest cluster is excluded from the summation.[39,40] The average ξ_{cluster} values are plotted for each system in Figure 4. As with $\xi_{\text{O-Z}}$, ξ_{cluster} shows a maximum at low χ_{M} before decaying to zero at $\chi_{\text{M}} = 1$ when all molecules exist on the same system-spanning cluster.

While $\xi_{\text{O-Z}}$ and ξ_{cluster} show qualitative similarities as they both stem from malonamide self-association, there are clear differences between the two properties across the composition range. At high DMDBPMA mole fraction, ξ_{cluster} is consistently smaller than $\xi_{\text{O-Z}}$. This results primarily from the DMDBPMA cluster connectivity definition, which produces edges between weakly interacting malonamides, merging them into the system-spanning cluster at high concentration, reducing the correlation length. Also apparent is that the maximum value of ξ_{cluster} is larger than the maximum of $\xi_{\text{O-Z}}$. This is primarily because ξ_{cluster} diverges (or, would for an infinitely large system) with the divergence in the mean cluster size at the percolation threshold.[35] Meanwhile, $\xi_{\text{O-Z}}$ simply passes through a maximum for an isotherm at $T > T_C$ and only diverges along the critical isotherm. Therefore, above T_C, while ξ_{cluster} would always diverge at some concentration along the isotherm, $\xi_{\text{O-Z}}$ does not, with the strength of its maxima determined by the distance of the isotherm from T_C.

While $\xi_{\text{O-Z}}$ and ξ_{cluster} both contain information that link a separations system to its location on the phase diagram, their relationship to the composition is different. The mole fractions at which the Widom and percolation lines intersect the compositional isotherm are not expected to be the same. Generally, the percolation line—the locus of percolation thresholds for a given definition of connectivity, the choice of which is arbitrary for continuum systems—depends on the connectivity definition and is not generally coincident with the Widom line and does not necessarily intersect the phase boundary at the critical point.[41,42] Rather, we might expect the isotherm to cross the percolation line at lower DMDBPMA mole fraction, as illustrated schematically in Figure 1, based on the percolation line for the 3D Ising model.[43]

This study has significant implications for the conventional understanding of several aspects of LLE organic phases. The scattering and cluster analysis both indicate that the malonamide concentrations fluctuations captured by $\xi_{\text{O-Z}}$ stem from the slow decay of solution inhomogeneity away from the critical point of the binary mixture rather than the formation of reverse micellar-like aggregates. This demonstrates that colloidal interpretations of the organic phase structure[7] are, for this system, neither appropriate nor necessary to describe the classical Ornstein-Zernike behavior at low-q.[44,45] Instead, we propose a fundamentally different origin for the dominant solution structure: dipole-driven self-association of DMDBPMA produces aggregates qualitatively comparable to clustering with the 3D Ising model. We expect this behavior to persist for the more lipophilic malonamides used in conventional LLE process. For example, we find that structure of dry (water-free) 0.5 M DMDBTDMA in n-dodecane (experimental data from ref. 13) is likewise dominated by Ornstein-Zernike-like behavior, as shown with a low-q fit in Figure S5. The fitted correlation length, plotted in Figure 4, is smaller than observed for DMDBPMA, as might be expected for the more lipophilic extractant having a lower T_C.

Overall, this suggests understanding the role of critical fluctuations is essential to relating LLE systems variables to organic phase structure and phase behavior. Generally, upon

approaching the liquid-liquid phase boundary along a compositional variable such as metal or acid concentration, the characteristic length scales observed in the organic phase increase, often substantially. Rather than indicating the growth in size of reverse micellar structures, as this behavior is typically interpreted, the critical behavior of the system may be driving the long-range concentration fluctuations as approaching the phase boundary naturally brings the system closer to the critical point. Attributing low-q electron density fluctuations to critical behavior could explain certain notably unphysical results from colloidal model fitting.[10,46–48]

As the Ornstein-Zernike scattering is generic, it does not preclude any specific nanostructural motif. When system complexity is increased and additional components or hierarchical structuring[11] are introduced into the organic phase, a physical interpretation of the critical fluctuations may not be obvious. Rather than mesostructure resulting from critical fluctuations of single malonamide units, as observed here, any potential micelle-like nanostructures may instead represent those structural units. In that case, critical fluctuations could correspond to aggregation of those units. Recently, Sheyfer et al. reported that the critical behavior of a malonamide/n-dodecane organic phase containing extracted water, nitric acid and lanthanide nitrate salts was consistent with a pseudo-binary order parameter having a single diverging length scale.[49] This order parameter is presumed to be analogous to the composition variable χ_{M} used here, with the additional compositional complexity impacting the location of the critical point but not the number of compositional degrees of freedom of the critical fluctuations. Sheyfer et al. also reported that the LLE organic phase is consistent with the 3D Ising universality class: in addition to capturing the clustering behavior across the range of χ_{M} as reported here, the 3D Ising model also defines the critical exponents of these organic phases, furthering its potential as a robust and simplified model for studying the organic phase. Overall, given the proximity of many LLE processes to their respective critical points—especially upon loading with aqueous components[49,50]—we broadly expect critical behavior to play a vastly more significant role than previously understood in the

structure of LLE organic phases.

Acknowledgments

We gratefully acknowledge support from a Physical Sciences Directorate Early Investigator Award from Argonne National Laboratory (MJS) and from DOE Office of Science, Office of Basic Energy Sciences, Materials Science and Engineering (GBS), both under US Department of Energy Contract No. DE-AC02-06CH11357. We further acknowledge the computing resources provided on Bebop, a high-performance computing cluster operated by the Laboratory Computing Resource Center at Argonne National Laboratory, under the same contract number.

Supporting Information

Computational details for molecular dynamics and Ising model, RDFs from simulation, and additional SAXS profiles including experimental data showing Ornstein-Zernike fits.

References

(1) Rydberg, J.; Cox, M.; Musikas, C.; Choppin, G. *Solvent Extraction Principles and Practices*, 2nd ed.; Marcel Dekker: New York, 2004.

(2) Zemb, T.; Bauer, C.; Bauduin, P.; Belloni, L.; Dejugnat, C.; Diat, O.; Dubois, V.; Dufreche, J.; Dourdain, S.; Duvail, M., et al. Recycling Metals by Controlled Transfer of Ionic Species between Complex Fluids: En Route to "Ienaics". *Colloid. Polym. Sci.* **2015**, *293*, 1–22.

(3) Bourgeois, D.; El Maangar, A.; Dourdain, S. Importance of Weak Interactions in the

Formulation of Organic Phases for Efficient Liquid/Liquid Extraction of Metals. *Curr. Op. Coll. Int. Sci.* **2020**, *46*, 36–51.

(4) Poirot, R.; Le Goff, X.; Diat, O.; Bourgeois, D.; Meyer, D. Metal Recognition Driven by Weak Interactions: A Case Study in Solvent Extraction. *ChemPhysChem* **2016**, *17*, 2112–2117.

(5) Špadina, M.; Bohinc, K. Multi-scale Modelling of Solvent Extraction and the Choice of Reference State: Mesoscopic Modelling as a Bridge between Nanoscale and Chemical Engineering. *Curr. Op. Coll. Int. Sci.* **2020**, *46*, 94–113.

(6) Knight, A. W.; Qiao, B.; Chiarizia, R.; Ferru, G.; Forbes, T.; Ellis, R. J.; Soderholm, L. Subtle Effects of Aliphatic Alcohol Structure on Water Extraction and Solute Aggregation in Biphasic Water/n-Dodecane. *Langmuir* **2017**, *33*, 3776–3786.

(7) Testard, F.; Zemb, T.; Bauduin, P.; Berthon, L. *Ion Exchange and Solvent Extraction: A Series of Advances*; CRC Press: Boca Raton, 2009; Vol. 19; Chapter Third-Phase Formation in Liquid/Liquid Extraction: A Colloidal Approach, pp 381–428.

(8) Chiarizia, R.; Jensen, M.; Borkowski, M.; Ferraro, J.; Thiyagarajan, P.; Littrell, K. Third Phase Formation Revisited: The U(VI), HNO_3, TBP, n-Dodecane System. *Solv. Extr. Ion Exch.* **2003**, *21*, 1–27.

(9) Chiarizia, R.; Nash, K.; Jensen, M.; Thiyagarajan, P.; Littrell, K. Application of the Baxter Model for Hard Spheres with Surface Adhesion to SANS Data for the U(VI)-HNO_3, TBP-n-Dodecane System. *Langmuir* **2003**, *19*, 9592–9599.

(10) Ellis, R. J.; Antonio, M. R. Coordination Structures and Supramolecular Architectures in a Cerium (III)–Malonamide Solvent Extraction System. *Langmuir* **2012**, *28*, 5987–5998.

(11) Motokawa, R.; Kobayashi, T.; Endo, H.; Mu, J.; Williams, C. D.; Masters, A. J.; Antonio, M. R.; Heller, W. T.; Nagao, M. A Telescoping View of Solute Architectures in a Complex Fluid System. *ACS Cent. Sci.* **2018**, *5*, 85–96.

(12) Ferru, G.; Reinhart, B.; Bera, M. K.; Olvera de la Cruz, M.; Qiao, B.; Ellis, R. J. The Lanthanide Contraction Beyond Coordination Chemistry. *Chem. Eur. J.* **2016**, *22*, 6899–6904.

(13) Servis, M. J.; Piechowicz, M.; Shkrob, I. A.; Soderholm, L.; Clark, A. E. Amphiphile Organization in Organic Solutions: An Alternative Explanation for Small-Angle X-ray Scattering Features in Malonamide/Alkane Mixtures. *J. Phys. Chem. B* **2020**, *124*, 10822–10831.

(14) Nishikawa, K.; Morita, T. Inhomogeneity of Molecular Distribution in Supercritical Fluids. *Chem. Phys. Lett.* **2000**, *316*, 238–242.

(15) Morita, T.; Kusano, K.; Ochiai, H.; Saitow, K.-i.; Nishikawa, K. Study of Inhomogeneity of Supercritical Water by Small-angle X-ray Scattering. *J. Chem. Phys.* **2000**, *112*, 4203–4211.

(16) Raju, M.; Banuti, D. T.; Ma, P. C.; Ihme, M. Widom Lines in Binary Mixtures of Supercritical Fluids. *Sci. Rep.* **2017**, *7*, 1–10.

(17) Brazhkin, V.; Fomin, Y. D.; Ryzhov, V.; Tareyeva, E.; Tsiok, E. True Widom Line for a Square-well System. *Phys. Rev. E* **2014**, *89*, 042136.

(18) Roth, R. Solvent-Mediated Interactions Close to the Fisher–Widom Line. *J. Phys. Chem. B* **2017**, *122*, 3556–3561.

(19) Luo, J.; Xu, L.; Lascaris, E.; Stanley, H. E.; Buldyrev, S. V. Behavior of the Widom Line in Critical Phenomena. *Phys. Rev. Lett.* **2014**, *112*, 135701.

(20) Xu, L.; Kumar, P.; Buldyrev, S. V.; Chen, S.-H.; Poole, P. H.; Sciortino, F.; Stanley, H. E. Relation between the Widom Line and the Dynamic Crossover in Systems with a Liquid–Liquid Phase Transition. *Proc. Nat. Acad. Sci.* **2005**, *102*, 16558–16562.

(21) Hestand, N. J.; Skinner, J. Perspective: Crossing the Widom Line in No Man's Land: Experiments, Simulations, and the Location of the Liquid-Liquid Critical Point in Supercooled Water. *J. Chem. Phys.* **2018**, *149*, 140901.

(22) Moore, E. B.; Molinero, V. Growing Correlation Length in Supercooled Water. *J. Chem. Phys.* **2009**, *130*, 244505.

(23) Abascal, J. L.; Vega, C. Widom Line and the Liquid–Liquid Critical Point for the TIP4P/2005 Water Model. *J. Chem. Phys.* **2010**, *133*, 234502.

(24) Kim, K. H.; Späh, A.; Pathak, H.; Perakis, F.; Mariedahl, D.; Amann-Winkel, K.; Sellberg, J. A.; Lee, J. H.; Kim, S.; Park, J., et al. Maxima in the Thermodynamic Response and Correlation Functions of Deeply Supercooled Water. *Science* **2017**, *358*, 1589–1593.

(25) Franzese, G.; Stanley, H. E. The Widom Line of Supercooled Water. *J. Phys. Cond. Matt.* **2007**, *19*, 205126.

(26) Greer, S. C. Liquid-Liquid Critical Phenomena. *Acc. Chem. Res.* **1978**, *11*, 427–432.

(27) Greer, S. C.; Moldover, M. R. Thermodynamic Anomalies at Critical Points of Fluids. *Ann. Rev. Phys. Chem.* **1981**, *32*, 233–265.

(28) Bauduin, P.; Testard, F.; Berthon, L.; Zemb, T. Relation between the Hydrophile/Hydrophobe Ratio of Malonamide Extractants and the Stability of the Organic Phase: Investigation at High Extractant Concentrations. *Phys. Chem. Chem. Phys.* **2007**, *9*, 3776–3785.

(29) Dozol, H.; Berthon, C. Characterisation of the Supramolecular Structure of Malonamides by Application of Pulsed Field Gradients in NMR Spectroscopy. *Phys. Chem. Chem. Phys.* **2007**, *9*, 5162–5170.

(30) Zhang, X.; Patel, L.; Beckwith, O.; Schneider, R.; Weeden, C.; Kindt, J. Extracting Aggregation Free Energies of Mixed Clusters from Simulations of Small Systems: Application to Ionic Surfactant Micelles. *J. Chem. Theory Comp.* **2017**, *13*, 5195–5206.

(31) Servis, M.; Wu, D.; Braley, J. Network Analysis and Percolation Transition in Hydrogen Bonded Clusters: Nitric Acid and Water Extracted by Tributyl Phosphate. *Phys. Chem. Chem. Phys.* **2017**, *19*, 11326–11339.

(32) Požar, M.; Lovrinčević, B.; Zoranić, L.; Primorać, T.; Sokolić, F.; Perera, A. Microheterogeneity versus Clustering in Binary Mixtures of Ethanol with Water or Alkanes. *Phys. Chem. Chem. Phys.* **2016**, *18*, 23971–23979.

(33) Qiao, B.; Littrell, K. C.; Ellis, R. Liquid Worm-like and Proto-Micelles: Water Solubilization in Amphiphile-Oil Solutions. *Phys. Chem. Chem. Phys.* **2018**,

(34) Vatin, M.; Duvail, M.; Guilbaud, P.; Dufrêche, J.-F. Thermodynamics of Malonamide Aggregation Deduced from Molecular Dynamics Simulations. *J. Phys. Chem. B* **2021**,

(35) Stauffer, D.; Aharony, A. *Introduction to Percolation Theory*; CRC press, 2018.

(36) Tanford, C. Thermodynamics of Micelle Formation: Prediction of Micelle Size and Size Distribution. *Proc. Nat. Acad. Sci.* **1974**, *71*, 1811–1815.

(37) Stanley, H. E. *Introduction to Phase Transitions and Critical Phenomena*; Oxford Univ. Press, 1971.

(38) Fisher, M. E. Renormalization Group Theory: Its Basis and Formulation in Statistical Physics. *Rev. Mod. Phys.* **1998**, *70*, 653.

(39) Lee, S. B.; Torquato, S. Monte Carlo study of Correlated Continuum Percolation: Universality and Percolation Thresholds. *Phys. Rev. A* **1990**, *41*, 5338.

(40) Geiger, A.; Stanley, H. E. Tests of Universality of Percolation Exponents for a Three-dimensional Continuum System of Interacting Waterlike Particles. *Phys. Rev. Lett.* **1982**, *49*, 1895.

(41) Campi, X.; Krivine, H.; Sator, N. Percolation Line of Self-bound Clusters in Supercritical Fluids. *Physica A* **2001**, *296*, 24–30.

(42) Strong, S. E.; Shi, L.; Skinner, J. Percolation in Supercritical Water: Do the Widom and Percolation Lines Coincide? *J. Chem. Phys.* **2018**, *149*, 084504.

(43) Sator, N. Clusters in Simple Fluids. *Phys. Rep.* **2003**, *376*, 1–39.

(44) Almasy, L.; Turmine, M.; Perera, A. Structure of Aqueous Solutions of Ionic Liquid 1-butyl-3-methylimidazolium Tetrafluoroborate by Small-angle Neutron Scattering. *J. Chem. Phys. B* **2008**, *112*, 2382–2387.

(45) Schroer, W.; Triolo, A.; Russina, O. Nature of Mesoscopic Organization in Protic Ionic Liquid–Alcohol Mixtures. *J. Phys. Chem. B* **2016**, *120*, 2638–2643.

(46) Chiarizia, R.; Jensen, M. P.; Rickert, P. G.; Kolarik, Z.; Borkowski, M.; Thiyagarajan, P. Extraction of Zirconium Nitrate by TBP in n-Octane: Influence of Cation Type on Third Phase Formation According to the "Sticky Spheres" Model. *Langmuir* **2004**, *20*, 10798–10808.

(47) Plaue, J.; Gelis, A.; Czerwinski, K.; Thiyagarajan, P.; Chiarizia, R. Small-Angle Neutron Scattering Study of Plutonium Third Phase Formation in 30% TBP/HNO3/Alkane Diluent Systems. *Solv. Extr. Ion Exch.* **2006**, *24*, 283–298.

(48) Dourdain, S.; Špadina, M.; Rey, J.; Bohinc, K.; Pellet-Rostaing, S.; Dufrêche, J.-F.; Zemb, T. How Acidity Rules Synergism and Antagonism in Liquid–Liquid Extraction

by Lipophilic Extractants—Part I: Determination of Nanostructures and Free Energies of Transfer. *Solv. Extr. Ion Exch.* **2021**, 1–20.

(49) Sheyfer, D.; Zhang, Q.; Lal, J.; Loeffler, T.; Dufresne, E.; Sandy, A.; Narayanan, S.; Sankaranarayanan, S.; Szczygiel, R.; Maj, P., et al. Nanoscale Critical Phenomena in a Complex Fluid Studied by X-ray Photon Correlation Spectroscopy. *Phys. Rev. Lett.* **2020**, *125*, 125504.

(50) Ellis, R. Critical Exponents for Solvent Extraction Resolved Using SAXS. *J. Phys. Chem. B* **2014**, *118*, 315–322.